Water-floated Ultrathin P(NDI2OD-T2) Films with Majority Edge-on Orientation Throughout The Film

*Thomas Steckmann, Indunil Angunawela, Somayeh Kashani, Youqin Zhu, Masrur M. Nahid, Harald Ade, and Abay Gadisa**

T. Steckmann, I. Angunawela, S. Kashani, M. M. Nahid, H. Ade, and A. Gadisa

Department of Physics, Organic and Carbon Electronics Labs (ORaCEL), North Carolina State University, Raleigh, NC 27695, USA

E-mail: agdinku@ncsu.edu; abaygd@gmail.com

Y. Zhu

Technology Group Co., Ltd., Beijing 100176, China

Keywords. Water-processing, transistor, ultrathin, mobility, interface, edge-on, stacking

Ultrathin organic films (typically < 10 nm) attracted great attention due to not only their (semi)transparency but also their unique optoelectronic properties that benefit applications such as sensors and flexible electronics. At the core of that, achieving high mobility in an ultrathin film is essential for the efficient operation of relevant electronic devices. While the state of the art material systems e.g. P(NDI2OD-T2) aka N2200 can achieve high mobility in a thin film (typically > 20 nm), multitudinous challenges remain when an ultrathin film is processed with that material where the desired charge transport morphology within a preferred thickness needs to be achieved. Here, high electron mobility (a 10-fold increase compared to annealed spin-coated films) is reported in both the top and bottom-gate configuration OFETs comprising ultrathin N2200 films produced with a water-floating film transfer method. We use a range of characterization techniques to investigate these ultrathin films and their microstructure, and conclude that favorable edge-on polymer orientation at the top as well as throughout the ultrathin film thickness with improved π–π stacking coherence lengths resulted in this high mobility in N2200 ultrathin films, in stark contrast to the commonly observed microstructural gradient in spin-coated thin films. Our results provide new insight into the electronic and microstructural properties of thin films of organic semiconductors.

1. Introduction

The current generation of organic field-effect transistors (OFETs) is rapidly approaching performance standards that are required to realize functioning electronics devices. In particular, recent achievements of enhanced charge carrier mobility, current on/off ratio, improved stability, and acceptably small threshold voltages are important milestones in the quest for developing commercially viable OFETs.[1,2] While not likely to challenge the performance of silicon transistors in computing applications, OFETs offer unique advantages in applications such as flexible and wearable electronics,[3] and transparent or translucent devices in display technology.[4] Each of these applications can be addressed by focusing not only on the materials used to fabricate OFETs, but also the fabrication methods to prioritize the large area and efficient fabrication of OFETs in the ultrathin (less than 10 nm) regime. Ultrathin devices can offer numerous advantages: reducing the thickness of the channel increases the elastic modulus of the OFET in wearable and flexible electronics,[3] while their large surface area in contact with the environment makes them excellent candidates to develop highly sensitive gas and chemical sensors.[5] In OFETs with an ultrathin active layer, the whole transistor channel can easily be accessed by an external environment (gas or chemical), which significantly improves the diffusion of the analytes through the organic active layer to the sensing interface (the semiconductor/dielectric interface), leading to high sensitivity.[5] Additionally, due to the scarcity of transparent conjugated semiconducting polymers, a viable approach to fabricate transparent devices is to reduce the amount of available light-absorbing material by reducing the film thickness. Thinner devices necessarily use less material, which further reduces the fabrication cost of OFETs and makes them more appealing for industrial adoption and more accessible for everyday electronics.

To realize ultrathin films, one of the best approaches is the floating film transfer method (FTM), also known as air-liquid interfacial self-assembly[6,7] or the spontaneous spreading phenomenon,[8] which takes advantage of the spreading coefficient between a solvent and liquid substrate to spontaneously spread a thin, uniform polymer film across the surface of the substrate (see Figure S1). Once dried, the film can be directly transferred to a substrate. Prior works that primarily focused on manipulating the fabrication conditions of the films have successfully demonstrated the viability of the method both as a highly scalable method capable of roll-to-roll fabrication,[9] and the ability to control film characteristics and self-annealing by varying the fabrication conditions.[10–12]

In general, mobilities exceeding 20 cm^2/Vs were reported for OFETs employing well-controlled film morphology.[13–15] To achieve high OFET performance, it is critical to acquire optimized film microstructure near the polymer/dielectric interface. Specifically, edge-on preferential crystal orientation[16] and substantially high coherence length[17] are critically preferred to realize efficient charge transport across the transistor channel. An edge-on orientation can be achieved through controlled film processing protocols such as solvent treatment,[18–20] thermal annealing[21] unidirectional solution processing,[22–24] and solvent-assisted friction transfer methods.[25] Using the Langmuir-Schäfer (LS) film casting method, S. Fabiano *et al.* demonstrated monolayer polymer OFETs showing preferentially edge-on orientation and thickness-dependent mobility.[26] The later authors, using the high-mobility semiconducting n-type polymer poly{[N,N9-bis(2-octyl dodecyl)-naphthalene-1,4,5,8-bis(dicarboximide)-2,6-diyl]-alt-5,59-(2,29-bithiophene)} (P(NDI2OD-T2), Polyera ActivInk N2200)[27], have successfully analyzed the performance of N2200/PMMA top-gate bottom-contact (TGBC) OFETs with only a single monolayer,[26,28] and subsequent work has demonstrated that LS film fabrication only allows for the creation of film molecular layers which are confined to 2D charge transport within only the interfacial, mostly edge-on polymer molecular layer.[29] According to the work of A. Salleo *et al*., melt annealing of N2200 films,[30] lead to a predominantly edge-on orientation and a two-fold increase in crystallinity in the bulk though this change is uncorrelated with transistor operation, indicating a different morphology is maintained at the organic/insulator interface. The highest mobilities in N2200 have been observed in top-gate bottom-contact device configurations, including the observation of record mobilities over 1 cm^2/Vs,[31] while bottom-gate bottom-contact (BGBC) devices often suffer from significant performance drops. This interface-dependent transport is mostly attributed to the vertical gradient in polymer orientation.[32]

Herein, we analyze the charge transport properties and thickness control of N2200 transistors fabricated using FTM. The results of this study indicate ultrathin N2200 OFETs exhibit high mobilities both in the top and bottom gate OFETs. This result is contrasted with prior attempts at fabricating films *via* sequential monolayer deposition of the Langmuir-Schaeffer method where the 2D charge transport in a bilayer LS film was detrimental to electron mobility.[26] In comparison, FTM allows for fabricating ultrathin films with no such mobility handicap. Indeed, FTM films have comparable to or even exceeded the mobility typically recorded in spin-coated devices. Our finding highlights the possibility of achieving high performance in thin-film electronics, by exploring the role of thickness on molecular orientation and order.

2. Results and Discussions

2.1 Film Formation

Films of N2200 were formed by drop-casting 10 to 50 μl of a warm polymer solution in p-xylene onto room temperature water (See Supporting Figure S1). P-xylene is relatively insoluble in water and has a high spreading coefficient among good solvents for N2200.[31,33]. The high spreading coefficient and relatively slow evaporation ensure a uniform spreading of polymer solution across the water surface before solvent evaporation is complete. It is also noted that warm polymer solution (70°C) slows down polymer aggregation preceding film formation. Films cast from solvents such as chloroform, dichlorobenzene, and 1,2-dichlorobenzene lack continuity and uniformity. Full processing details can be found in the experimental section.

Films were transferred to either glasses or transistor substrates for investigating their optical, microstructural, and electrical properties. Ultrathin films of N2200, down to a few molecular layers of thicknesses of approximately ~2.6 nm as in Figure S2, were produced. Film thickness was controlled *via* manipulation of three parameters in the FTM film formation: the solution concentration, the volume of the deposited solution, and the surface area of the liquid substrate determined by the area of the container used for casting. Transferring films from the water surface to substrates requires the usage of a highly hydrophobic substrate to prevent intrusion of water onto the substrate: in these experiments, the substrates are treated with OTS (octadecyltrichlorosilane), which also has beneficial charge transport properties in transistors.[34]

2.2 OFET Charge Transport

The charge transport properties of the N2200 thin films were studied in both top-gate and bottom-gate bottom-contact OFETs. The current-voltage output characteristics of the transistors are displayed in Figures S3 and S4 in the supporting information. The electron mobility of the N2200 films is displayed in Figure 1 and Table 1. As inferred from Figure 1 and Table 1, better electron mobility is achieved in the ultrathin films while thicker films seem to reduce charge transport regardless of device configuration. In fact, the mobility of the thickest floated films (~30 nm) and the best spin-cast films are nearly the same in both TGBC and BGBC OFTEs. It is well known that BGBC OFETs give low mobility in N2200 films due to unfavorable material structure at the gate dielectric/N2200 interface.[24,31] Because of this

restriction, TGBC OFETs are often employed to characterize the charge transport of N2200. It is noted that the thick floated sample gives better mobility in TGBC transistors (Fig. 1b), which is consistent with literature reports.[31]

The mobility trend observed here is different from previous reports. N2200 films fabricated with the Langmuir-Schaefer method exhibited a decrease in mobility for thickness less than ~15 nm (5 monolayers) when characterized in TGBC device configuration.[26] An inverse correlation of OFET mobility with thickness was also observed for other polymers.[35–37] It is, therefore, quite interesting to observe that N2200 ultrathin films show high mobility irrespective of device configuration.

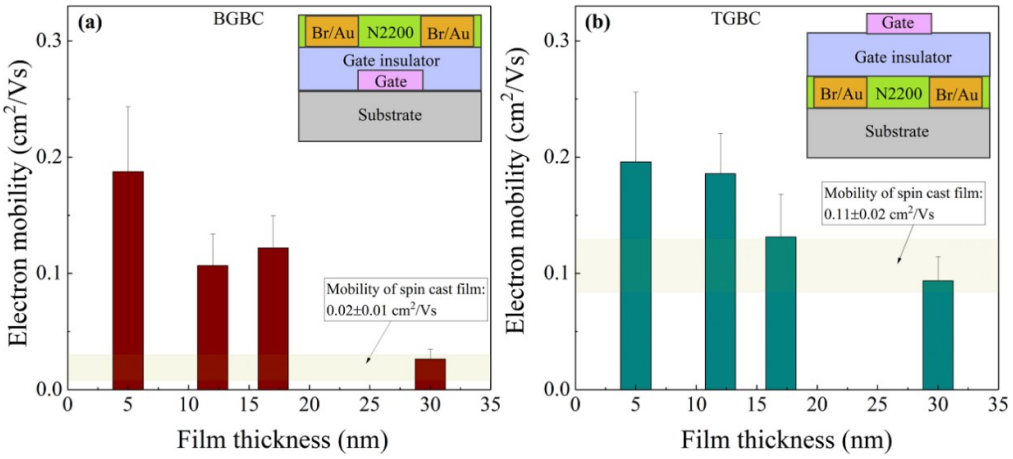

Figure 1. OFET mobility of (a) bottom-gate bottom-contact, and (b) top-gate bottom-contact devices as a function of the film thickness of floated films. The shaded areas show the mobility of 35 nm spin-cast films.

Table 1. The electron mobility of bottom-gate bottom-contact (BGBC) and top-gate bottom-contact (TGBC) OFETs.

OFET type	Film thickness (nm)	Mobility (cm^2/Vs)
BGBC	5	0.19
BGBC	12	0.11
BGBC	17	0.12
BGBC	30	0.03
TGBC	5	0.23
TGBC	12	0.19
TGBC	17	0.13
TGBC	30	0.09

2.3 **Bulk microstructure**

To get better insight into the molecular packing of the thin films, we analyzed the films using Grazing-Incidence Wide-Angle X-ray Scattering (GIWAXS).[38] The 2D GIWAXS patterns of the floated and spin-cast samples are shown in Figure 2a-c and their line cuts are displayed in Figure 2d and e. The 1D line-cuts of the ultrathin floated sample shows higher-order lamellar stacking in the out-of-plane direction, indicating a more edge-on orientation. The properties of the molecular packing were explored further by exploring their in-plane π–π stacking coherence length, which was obtained from fits (See Figure S5) of the GIWAXS line cuts. The coherence length (L_c) of the in-plane π–π stacking is found to be the highest in the ultrathin floated film as listed in Table 2. The absolute value of the L_c of the 5 nm film could be debatable since the overlapping peaks affect the accuracy of the peak fitting (Figure S5). However, the increasing trend of L_c with decreasing film thickness holds for the out-of-plane π–π stacking as inferred from Table 2, confirming the trend achieved in the in-plane direction. Moreover, as inferred from Table 1, the floated films show a lower π–π stacking distance in the in-plane direction, which is essential for better charge transport across the stacking direction.[39,40] A larger coherence length is indicative of a long-range molecular order, which is desired for efficient charge transport. A strong long-range in-plane order in ultrathin polymer films is rarely reported.[41]

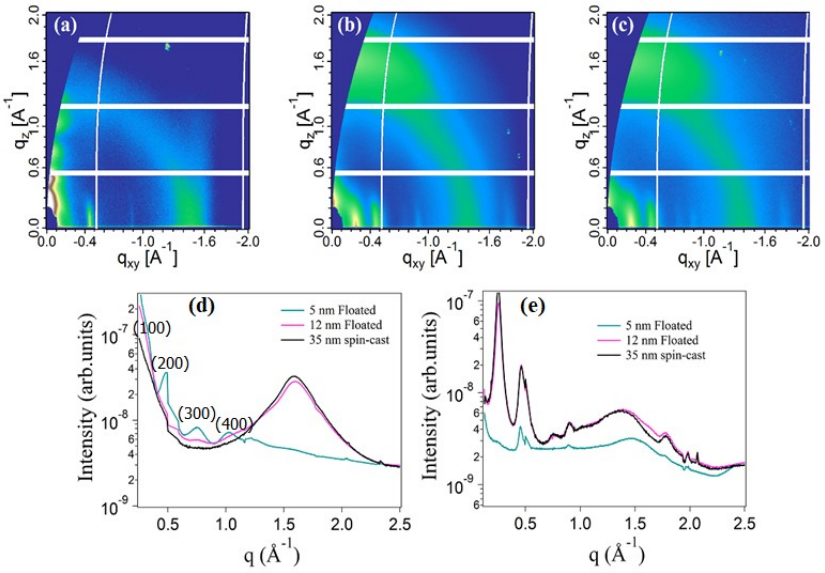

Figure 2. 2D GIWAXS patterns of (a) floated 5 nm, (b) floated 12 nm, and (c) spin-cast 35 nm films. Corresponding (d) out-of-plane, and (e) in-plane GIWAXS 1D line-cuts of floated and spin-cast films.

Table 2. The GIWAXS parameters of the in-plane π–π peak fittings of the films. (π–π stacking distance *d*, Coherence length L_c).

Film type	Thickness	In-plane π–π stacking		Out-of-plane π–π *stacking*	
	(nm)	*d* (Å)	L_c (Å)	*d* (Å)	L_c (Å)
Ultrathin floated	5	3.93	50	3.89	30
Thin floated	12	3.93	26	3.93	20
Spin cast	35	4.19	23	3. 95	19

The lamellar stacking and the π–π stacking in the 2D GIWAXS patterns were further analyzed using GIWAXS pole figure analysis (See Figure S6)[42] to understand the orientation distribution of the films. The edge-on (A_E) to face-on (A_F) orientation ratio (A_E/A_F) was obtained by integrating the pole figure intensity with reference to the 45^0 azimuthal angles to obtain the intensity of a particular orientation (See Figure 3) which is proportional to the population of that orientation. To obtain the A_E/A_F ratio, the isotropic fraction was subtracted from the pole figure intensities following the best practice in the literature.[42] As inferred from Figure 3, the ultrathin floated film (5 nm) is predominantly edge-on which is indicated by its significantly higher A_E/A_F ratio. It is noted that a thicker floated film exhibits an increased population of face-on orientation, and yet the spin-coated sample (35 nm) shows a relatively strong face-on orientation as determined from its low A_E/A_F ratio.

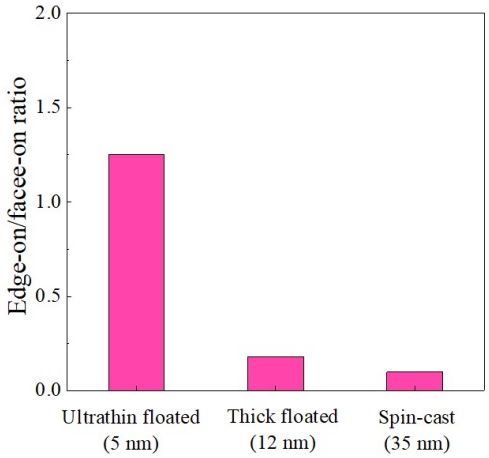

Figure 3. Edge-on to a face-on ratio (A_E/A_F) of the water-floated and spin-cast films.

2.4 Surface Morphology

Atomic force microscopy (AFM) images showing surface microstructural features of the floated films with varying thicknesses are displayed in Figure 4. As inferred from the AFM images, N2200 floated films form fibrillar-like structures on the surface of the film with some degree of orientation, which is typical for this material.[24,43] The polymer microstructures are more evident in the phase images (d–f), with anisotropic fiber distributions. The surface morphology of the 35 nm spin-cast film (See Supporting Figure S7) shows a close resemblance with the surface structure of the thick (30 nm) floated film.

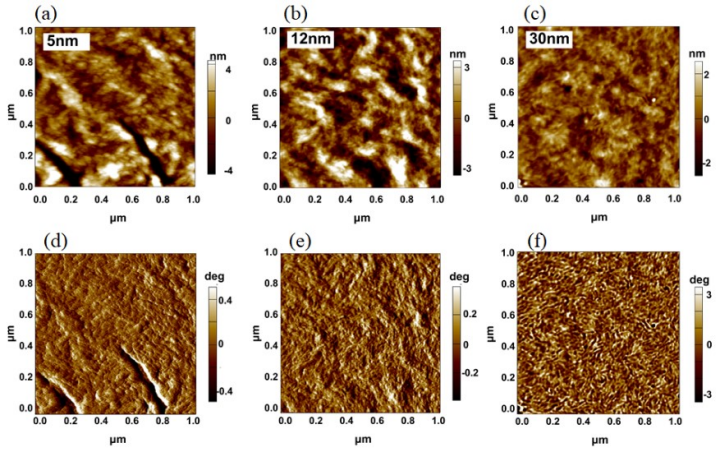

Figure 4: Topographic AFM height images of floated films of different thicknesses: (a), (b), and (c) are height images of 5, 12, and 30 nm thick films, respectively. Corresponding phase images of the 5, 12, and 30 nm are shown in (d), (e), and (f), respectively.

We made further analysis of fiber dimensions by analyzing the real-space length scales of the thin films using power spectral density (PSD) analysis of the AFM phase images. The peaks shown in the PSD data (Figure 5) are related to the real space periodicity[44] of the surface of the film. The observed difference in the PSD profile is indicative of a varying length scale in materials order.

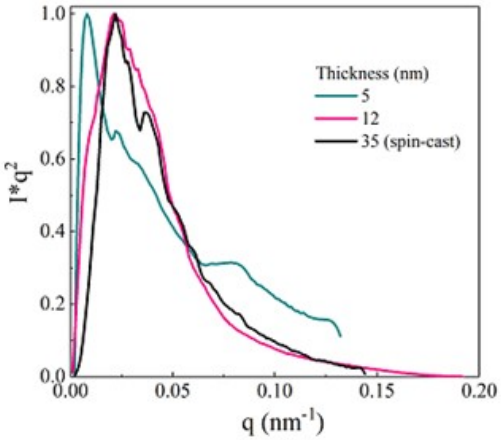

Figure 5. The PSD profiles as analyzed from the AFM phase images.

2.5 Optical Properties

The UV-vis absorption spectrum of N2200 floated and spin-cast films were characterized and depicted in Figure 5 and Figure S8. All films exhibit two distinct bands: the high-energy bands (near 3.2 eV), and the low-energy bands (1.75−1.77 eV), consistent with the literature.[45–49] According to the data presented in Figure 5 (a), the progression of the absorption spectra is dependent on film thickness particularly in high energy regions, which may be indicative of structural changes. A close look at the low energy peaks (Figure 5, (b)) shows that the ultrathin film reveals a broad shoulder peak (1.55−1.63 eV), which is ascribed to aggregated chain segments.[47] On the other hand, it is noted that the 35 nm spin-cast film the thickest floated sample (30 nm) exhibits similar optical properties.

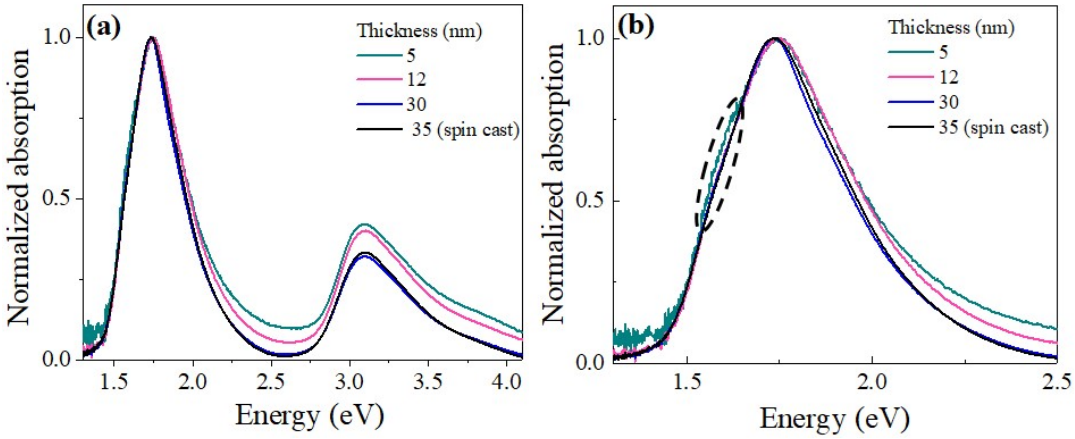

Figure 5. (a) The normalized absorption spectra of N2200 films. (b) The low energy band of the normalized absorption. The gray circle shows a vibration peak that is only clearly observed for the 5 nm film.

3. Correlating The Microstructural and Electrical Properties

According to the charge transport studies, high electron mobility can be achieved in ultrathin floated films both in TGBC and BGBC transistors. Interestingly, nearly 10-fold mobility can be achieved in BGBC devices utilizing ultrathin films compared to transistors with spin-coated films. The low mobility extracted from the BGBC N2200 transistor is a known long-standing problem for spin-casted films, and this limitation is ascribed to the preferential edge-on orientation of the polymer chains only at the air interface.[32] Indeed, the strong edge-on orientation of the 5 nm floated film correlates well with its high OFET mobility while the decreased edge-on orientation in thicker films (Figure 3) is accompanied by a drop in carrier mobility (Figure 1).

On the other hand, the π–π stacking coherence length is correlated with charge carrier mobility since it relates to the order of the aggregates.[50,51] Long-range order of aggregates improves charge transport by facilitating highly connected percolation pathways. According to the GIWAXS analysis (Table 2), the coherence length of the ultrathin floated film is improved compared to the 12 nm floated and spin-cast films. This is also consistent with the appearance of a shoulder peak in the optical transition of the ultrathin film (Figure 5 (b)), indicative of aggregate formation. Besides, the PSD data revealed a larger length scale in the thinner film implying a larger fiber spacing and long-range order, which is known to be a recipe for efficient OFET charge transport.[51] It is noted that though the spin-cast film shows clear and thicker fibers in AFM images (Figure S7) compared to the floated films, it gives comparatively lower charge mobility due to its lower order in its microstructures as witnessed in its small L_c as inferred from Table 2.

It can, therefore, be concluded that the preferred edge-on orientation together with the long-range order of the ultrathin floated samples has improved its device mobility. In addition, the comparatively high mobility of the ultrathin film regardless of OFET structure is indicative of the distribution of edge-on orientation throughout the film volume. The latter is a new observation for N2200. S. Fabiano *et al.* demonstrated high mobility in top-gate bottom-contact OFETs comprising a monolayer film of N2200 that is produced with the Langmuir-Schäfer deposition technique. They observed an increase in mobility as the number of layers increases, saturating with a mean value of 0.018 cm^2/Vs at about 9 nm (3 layers).[26] Our finding provides a means for the fabrication of ultrathin organic films characterized with efficient electrical properties due to an immediate realization of the desired film morphology. Moreover, our finding has an important implication for thin-film-based electronic devices. For example, in OFET chemical[5] and gas[52] sensors, ultrathin organic semiconductor films

enhance response time significantly due to improved analyte motion to the sensing interface, whereas increased mobility is essential to achieve high sensitivity. We, therefore, believe that this work provides a vital guideline for the further development of next-generation sensors, flexible and wearable electronics.

4. Conclusions

In this study, the electronic properties of ultrathin films of N2200 are explored in OFETs by considering films floated on the water surface. This research finds that ultrathin films (< 10 nm) give high electron mobility in both BGBC and TGBC OFETs, while increasing film thickness lowers mobility. Such drastic changes in charge transport in thicker films reflect changes in the film microstructural features such as orientation at the device interfaces regardless of film-forming protocols. The ultrathin films retain a dominantly edge-on orientation and ordered morphology throughout the film volume, thus giving enhanced mobility in OFET regardless of device architecture. This finding unveils a spontaneous formation of favorable film structure in polymer ultrathin films, which is crucial for developing transparent and flexible electronics.

5. EXPERIMENTAL DETAILS

Sample preparation: The OFET substrates include a heavily doped Si (500 μm), and a 300 nm thick layer of SiO2 as the gate dielectric. To fabricate the transistor testbeds, Br (10 nm)/Au (40 nm) contacts were evaporated on pre-patterned substrates. Dual gate transistor structures encompassing both bottom-gate, and bottom-contact and top-gate bottom-contact structures were fabricated to measure charge transport at both interfaces. Before casting the polymer films, the substrates were cleaned with DI-water acetone and isopropanol and subsequently treated with octadecyltrichlorosilane (OTS) to form a self-assembled monolayer following a previously used procedure.[51,53] The active layers were cast on water from a p-xylene solution and transferred to the transistor substrates by directly placing the substrates on the films. The results films were annealed at 110 °C in a nitrogen-filled glove box to dry the films. Film thicknesses were varied by changing solution concentration as well as the volume of solution dropped on the water substrate. To fabricate top-gated OFETs, CYTOP (Asahi Glass) was spin-coated on top of the N2200 films at 9000 rpm for 90 seconds resulting in a 500 nm dielectric layer. This was followed by annealing at 110 °C (4 h) before depositing a 40 nm thick Al gate through a shadow mask.

Measurements: The different characterization methods are listed below.

GIWAXS: Grazing-incidence wide-angle X-ray scattering (GIWAXS) measurements were conducted at the Advanced Light Source (ALS), Lawrence Berkeley National Laboratory, Berkeley, CA at the beamline 7.3.3. Data were acquired at the critical angle (0.130) of the film with a hard X-ray energy of 10 keV. X-ray irradiation time was 10-30 s, depending on the saturation level of the detector. The Beam Center was calibrated using AgBr powder and the sample-to-detector distance was about 330 mm. The π-π coherence lengths are estimated based on the Scherrer Equation (L=2πK/FWHM), where K=0.9 is the shape factor, and FWHM is the full width at half maximum of the (010) diffraction peaks.

AFM measurements: The AFM images were recorded using an Asylum research MFP-3D system in taping mode.

Absorption spectrum: The ex-situ UV-Vis spectra were recorded with Cary 60 spectrometer (Agilent). Devices were tested and relevant parameters were extracted from slopes to transfer curves in the saturation regime.

OFET I-V Characteristics: The OFETs were characterized by a Keithley 4200 Semiconductor Parameter Analyzer. The parameter analyzer was coupled with triaxial feedthroughs with a Janis probe station, where the test samples were placed in a turbo-pumped vacuum chamber (10^{-5} mbar). The device parameters were extracted from the transfer and output curves in the saturation regime.

Supporting Information

Supporting Information is available from the Wiley Online Library or the author.

Acknowledgments

The authors gratefully acknowledge the support from the U.S. Office of Naval Research (ONR, grant No. N000141712204) and the UNC General Administration Research Opportunity Initiative grant. X-ray data were acquired at beamline 11.0.1.2 and 7.3.3 at the Advanced Light Source, which is supported by the Director, Office of Science, Office of Basic Energy Sciences, of the U.S. Department of Energy under contract no. DE-AC02-05CH11231.

Received: ((will be filled in by the editorial staff))

Revised: ((will be filled in by the editorial staff))

Published online: ((will be filled in by the editorial staff))

References

[1] Y. Yao, H. Dong, F. Liu, T. P. Russell, W. Hu, *Adv. Mater.* **2017**, *29*, 1701251.

[2] P. Hu, X. He, H. Jiang, *InfoMat* **2021**, *3*, 613.

[3] X. Tao, V. Koncar, *Smart Text. Their Appl.* **2016**, 569.

[4] Y. Li, X. Guo, Z. Peng, B. Qu, H. Yan, H. Ade, M. Zhang, S. R. Forrest, *Proc. Natl. Acad. Sci.* **2020**, *117*, 21147.

[5] Y. Wang, J. Zhang, S. Zhang, J. Huang, *Polym. Int.* **2021**, *70*, 414.

[6] M. H. M. Cativo, D. K. Kim, R. A. Riggleman, K. G. Yager, S. S. Nonnenmann, H. Chao, D. A. Bonnell, C. T. Black, C. R. Kagan, S.-J. Park, *ACS Nano* **2014**, *8*, 12755.

[7] S. Oh, M. Yang, J. Bouffard, S. Hong, S.-J. Park, *ACS Appl. Mater. Interfaces* **2017**, *9*, 12865.

[8] Y. Sung, E.-Y. Shin, Y.-Y. Noh, J.-Y. Lee, *ACS Appl. Mater. Interfaces* **2020**, *12*, 25092.

[9] J. Noh, S. Jeong, J.-Y. Lee, *Nat. Commun.* **2016**, *7*, 12374.

[10] Y.-J. Kim, H.-T. Jung, C. W. Ahn, H.-J. Jeon, *Adv. Mater. Interfaces* **2017**, *4*, 1700342.

[11] Y.-J. Kim, K. Park, H.-T. Jung, C. W. Ahn, H.-J. Jeon, *Cryst. Growth Des.* **2018**, *18*, 1261.

[12] A. S. M. Tripathi, N. Kumari, S. Nagamatsu, S. Hayase, S. S. Pandey, *Org. Electron.* **2019**, *65*, 1.

[13] H.-R. Tseng, H. Phan, C. Luo, M. Wang, L. A. Perez, S. N. Patel, L. Ying, E. J. Kramer, T.-Q. Nguyen, G. C. Bazan, A. J. Heeger, *Adv. Mater.* **2014**, *26*, 2993.

[14] C. Luo, A. K. K. Kyaw, L. A. Perez, S. Patel, M. Wang, B. Grimm, G. C. Bazan, E. J. Kramer, A. J. Heeger, *Nano Lett.* **2014**, *14*, 2764.

[15] J. Yang, Z. Zhao, S. Wang, Y. Guo, Y. Liu, *Chem* **2018**, *4*, 2748.

[16] K. Bulgarevich, K. Sakamoto, T. Minari, T. Yasuda, K. Miki, M. Takeuchi, *Adv. Funct. Mater.* **2019**, *29*, 1905365.

[17] Z. Wang, X. Song, Y. Jiang, J. Zhang, X. Yu, Y. Deng, Y. Han, W. Hu, Y. Geng, *Adv. Sci.* **2019**, *6*, DOI 10.1002/ADVS.201902412.

[18] P. Yang, Y. Han, *Langmuir* **2009**, *25*, 9960.

[19] P. K.-H. Ho, L.-L. Chua, M. Dipankar, X. Y. Gao, D. C. Qi, A. T.-S. Wee, J.-F. Chang, R. H. Friend, *Adv. Mater.* **2007**, *19*, 215.

[20] M. Qian, Z. Song, G. Ding, Z. Hu, J. Liu, *RSC Adv.* **2019**, *9*, 28648.

[21] H. Yang, R. Zhang, L. Wang, J. Zhang, X. Yu, J. Liu, R. Xing, Y. Geng, Y. Han, *Macromolecules* **2015**, *48*, 7557.

[22] H. Sun, Q. Wang, J. Qian, Y. Yin, Y. Shi, Y. Li, *Semicond. Sci. Technol.* **2015**, *30*, 054001.

[23] A. S. M. Tripathi, M. Pandey, S. Sadakata, S. Nagamatsu, W. Takashima, S. Hayase, S. S. Pandey, *Appl. Phys. Lett.* **2018**, *112*, 123301.

[24] N. E. Persson, S. Engmann, L. J. Richter, D. M. DeLongchamp, *Chem. Mater.* **2019**, DOI 10.1021/ACS.CHEMMATER.9B00888.

[25] N. Kumari, M. Pandey, H. Syafutra, S. Nagamatsu, M. Nakamura, S. S. Pandey, *ACS Appl. Mater. Interfaces* **2020**, *12*, 55033.

[26] S. Fabiano, C. Musumeci, Z. Chen, A. Scandurra, H. Wang, Y.-L. Loo, A. Facchetti, B. Pignataro, *Adv. Mater.* **2012**, *24*, 951.

[27] S. F. W. Designed Research; S, S. P. W. Performed Research; S, S., *Proc. Natl. Acad. Sci*. **2015**, *112*, 2020.

[28] M. Li, D. K. Mangalore, J. Zhao, J. H. Carpenter, H. Yan, H. Ade, H. Yan, K. Müllen, P. W. M. Blom, W. Pisula, D. M. de Leeuw, K. Asadi, *Nat. Commun.* **2018**, *9*, 451.

[29] V. D'Innocenzo, A. Luzio, H. Abdalla, S. Fabiano, M. A. Loi, D. Natali, A. Petrozza, M. Kemerink, M. Caironi, *J. Mater. Chem. C* **2016**, *4*, 11135.

[30] J. Rivnay, R. Steyrleuthner, L. H. Jimison, A. Casadei, Z. Chen, M. F. Toney, A. Facchetti, D. Neher, A. Salleo, *Macromolecules* **2011**, *44*, 5246.

[31] M. M. Nahid, A. Welford, E. Gann, L. Thomsen, K. P. Sharma, C. R. McNeill, *Adv. Electron. Mater.* **2018**, *4*, 1700559.

[32] T. Schuettfort, L. Thomsen, C. R. McNeill, *J. Am. Chem. Soc.* **2013**, *135*, 1092.

[33] W. D. Harkins, A. Feldman, *J. Am. Chem. Soc.* **2002**, *44*, 2665.

[34] S. J. Kang, Y. Yi, C. Y. Kim, C. N. Whang, T. A. Callcott, K. Krochak, A. Moewes, G. S. Chang, *Appl. Phys. Lett.* **2005**, *86*, 232103.

[35] S. Joshi, S. Grigorian, U. Pietsch, P. Pingel, A. Zen, D. Neher, U. Scherf, *Macromolecules* **2008**, *41*, 6800.

[36] H. Jia, S. Gowrisanker, G. K. Pant, R. M. Wallace, B. E. Gnade, *J. Vac. Sci. Technol. A Vacuum, Surfaces, Film.* **2006**, *24*, 1228.

[37] D. Khim, G.-S. Ryu, W.-T. Park, H. Kim, M. Lee, Y.-Y. Noh, *Adv. Mater.* **2016**, *28*, 2752.

[38] A. Hexemer, W. Bras, J. Glossinger, E. Schaible, E. Gann, R. Kirian, A. MacDowell, M. Church, B. Rude, H. Padmore, *J. Phys. Conf. Ser.* **2010**, *247*, 12007.

[39] M. Bajpai, R. Srivastava, R. Dhar, R. S. Tiwari, *Mater. Sci. Eng. B* **2016**, *212*, 62.

[40] J. M. Szarko, J. Guo, Y. Liang, B. Lee, B. S. Rolczynski, J. Strzalka, T. Xu, S. Loser, T.

J. Marks, L. Yu, L. X. Chen, *Adv. Mater.* **2010**, *22*, 5468.

[41] M. Li, D. K. Mangalore, J. Zhao, J. H. Carpenter, H. Yan, H. Ade, H. Yan, K. Müllen, P. W. M. Blom, W. Pisula, D. M. de Leeuw, K. Asadi, *Nat. Commun.* **2018**, *9*, 451.

[42] K. A. Page, A. Kusoglu, C. M. Stafford, S. Kim, R. J. Kline, A. Z. Weber, *Nano Lett.* **2014**, *14*, 2299.

[43] J. Liu, L. Qiu, R. Alessandri, X. Qiu, G. Portale, J. Dong, W. Talsma, G. Ye, A. A. Sengrian, P. C. T. Souza, M. A. Loi, R. C. Chiechi, S. J. Marrink, J. C. Hummelen, L. J. A. Koster, *Adv. Mater.* **2018**, *30*, 1704630.

[44] S. J. Fang, S. Haplepete, W. Chen, C. R. Helms, H. Edwards, *J. Appl. Phys.* **1997**, *82*, 5891.

[45] Y. Yan, Y. Liu, Q. Zhang, Y. Han, *Front. Chem.* **2020**, *8*, 394.

[46] J. R. Moore, S. Albert-Seifried, A. Rao, S. Massip, B. Watts, D. J. Morgan, R. H. Friend, C. R. McNeill, H. Sirringhaus, *Adv. Energy Mater.* **2011**, *1*, 230.

[47] R. Steyrleuthner, M. Schubert, I. Howard, B. Klaumünzer, K. Schilling, Z. Chen, P. Saalfrank, F. Laquai, A. Facchetti, D. Neher, *J. Am. Chem. Soc.* **2012**, *134*, 18303.

[48] K. G. Jespersen, W. J. D. Beenken, Y. Zaushitsyn, A. Yartsev, M. Andersson, T. Pullerits, V. Sundström, *J. Chem. Phys.* **2004**, *121*, 12613.

[49] G. Wen, X. Zou, R. Hu, J. Peng, Z. Chen, X. He, G. Dong, W. Zhang, *RSC Adv.* **2021**, *11*, 20191.

[50] R. Di Pietro, T. Erdmann, J. H. Carpenter, N. Wang, R. R. Shivhare, P. Formanek, C. Heintze, B. Voit, D. Neher, H. Ade, A. Kiriy, *Chem. Mater.* **2017**, *29*, 10220.

[51] I. Angunawela, M. M. Nahid, M. Ghasemi, A. Amassian, H. Ade, A. Gadisa, *ACS Appl. Mater. Interfaces* **2020**, *12*, 26239.

[52] L. Li, P. Gao, M. Baumgarten, K. Müllen, N. Lu, H. Fuchs, L. Chi, *Adv. Mater.* **2013**, *25*, 3419.

[53] X. Xue, G. Chandler, X. Zhang, R. Joseph Kline, Z. Fei, M. Heeney, P. J. Diemer, O. D. Jurchescu, Brendan T. O'Connor, *ACS Appl. Mater. Interfaces* **2015**, *7*, 26726.

Structure–property relationships of P(NDI2OD-T2) thin films are studied. Transistors with ultrathin films (floated on water) show high electron mobility regardless of transistor configuration. GIWAXS analysis reveals that ultrathin films are dominated by edge-on orientation while thicker films mostly assume face-on orientation at the transistor interface. Besides, the ultrathin films exhibit better long-range order, which enhances transport.

T. Steckmann, I. Angunawela, S. Kashani, Y. Zhu, M. M. Nahid, H. Ade, and A. Gadisa *

Water-floated Ultrathin P(NDI2OD-T2) Films with Majority Edge-on Orientation Throughout The Film

ToC figure ((Please choose one size: 55 mm broad × 50 mm high **or** 110 mm broad × 20 mm high. Please do not use any other dimensions))

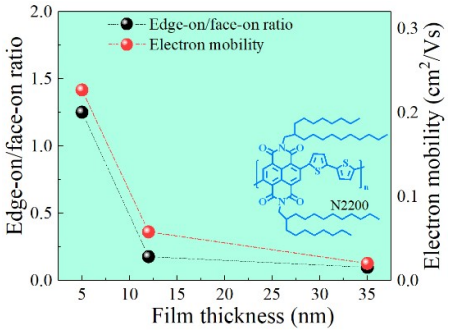

Supporting Information

Water-floated Ultrathin P(NDI2OD-T2) Films with Majority Edge-on Orientation Throughout The Film

Thomas Steckmann, Indunil Angunawela, Somayeh Kashani, Youqin Zhu, Masrur M. Nahid, Harald Ade, and Abay Gadisa *

T. Steckmann, I. Angunawela, S. Kashani, M. M. Nahid, H. Ade, and A. Gadisa

Department of Physics, Organic and Carbon Electronics Labs (ORaCEL), North Carolina State University, Raleigh, NC 27695, USA

E-mail: agdinku@ncsu.edu; abaygd@gmail.com

Y. Zhu

Technology Group Co., Ltd., Beijing 100176, China

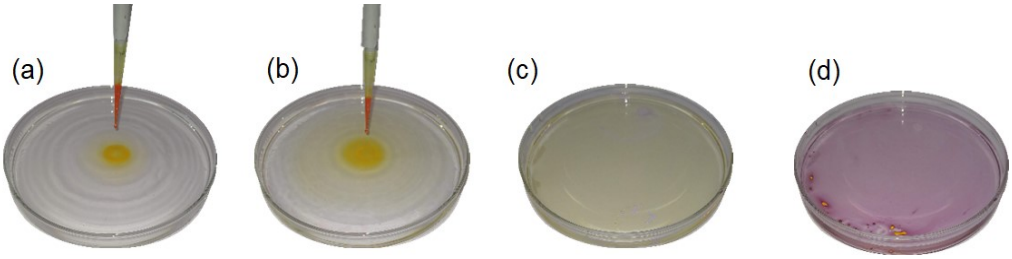

Figure S1. Film formation behavior of a wafer sized ~50 nm thick P3HT film (for visibility): (a) A polymer solution in p-Xylene is dropped onto the surface of deionized water. (b) For solutions with a spreading coefficient $S > 0$, the solution spontaneously spreads across the water surface. (c-d) The solution slowly evaporates, leaving behind a polymer thin film suspended on the surface. Deposition of thick films is bounded above by the elasticity of the film and poor uniformity due to slight variations in solvent evaporation rates across the surface of the film.

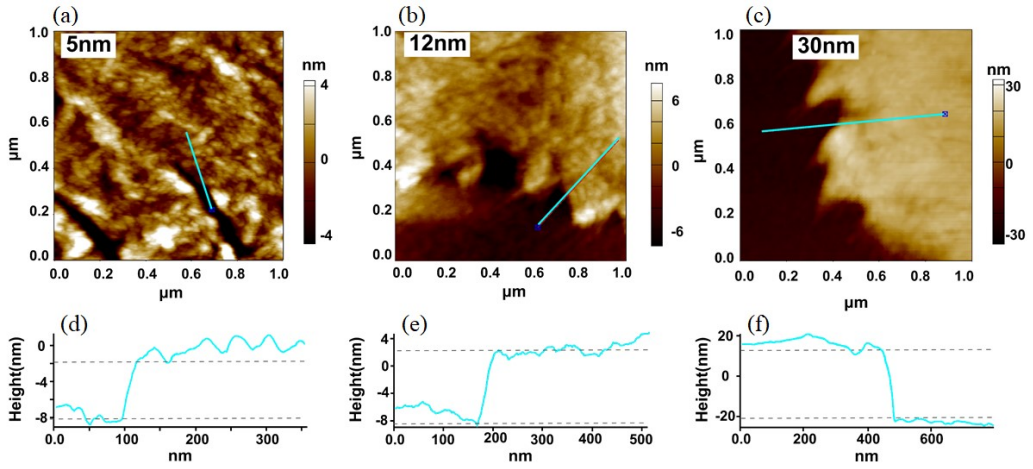

Figure S2**:** AFM height images of floated films of thicknesses (a) 5 nm, (b) 12 nm, and (c) 30 nm. Corresponding line cuts for the 5, 12, and 30 nm films are shown in (d), (e), and (f), respectively.

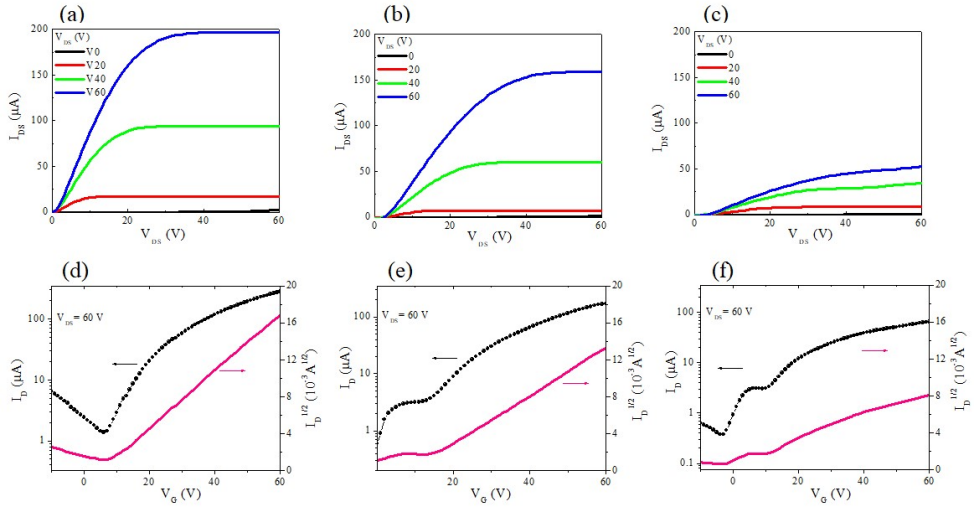

Figure S3: Output characteristics of the BGBC OFETS with floated N2200 films of thicknesses (a) 5 nm, (b) 12 nm, and (c) 30 nm. Corresponding transfer characteristics of the 5, 12, and 30 nm films are shown in (d), (e), and (f), respectively.

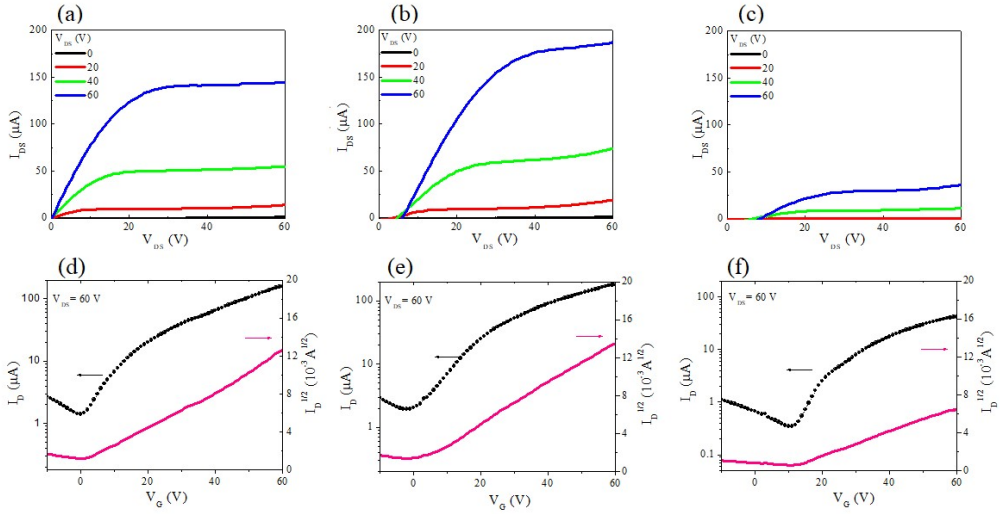

Figure S4: Output characteristics of the TGBC OFETS with floated N2200 films of thicknesses (a) 5 nm, (b) 12 nm, and (c) 30 nm. Corresponding transfer characteristics of the 5, 12, and 30 nm films are shown in (d), (e), and (f), respectively.

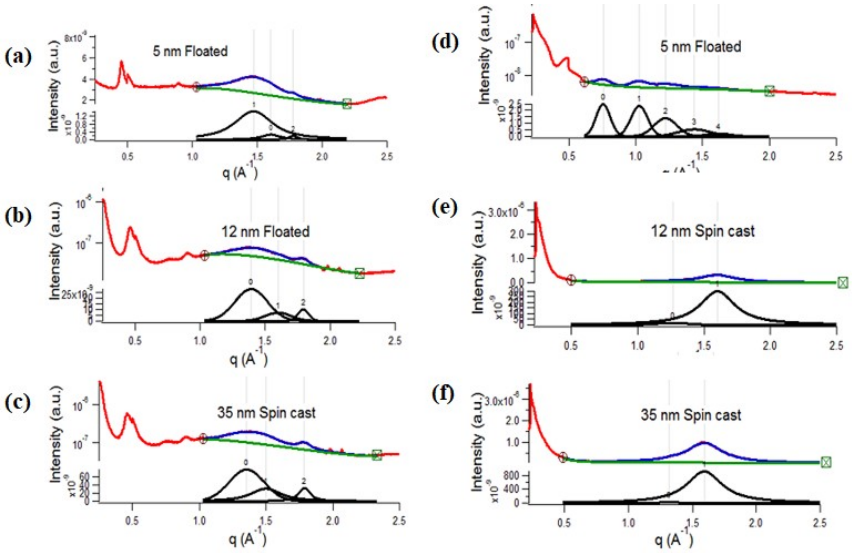

Figure S5: GIWAXS peak fitting of the in-plane line-cuts of the (a) floated 5 nm, (b) floated 12 nm, and (c) spin-cast 35 nm films. Corresponding GIWAXS peak fitting of the out-of-plane line-cuts of the floated 5 nm, floated 12 nm, and spin-cast 35 nm films are shown in (d), (e), and (f), respectively.

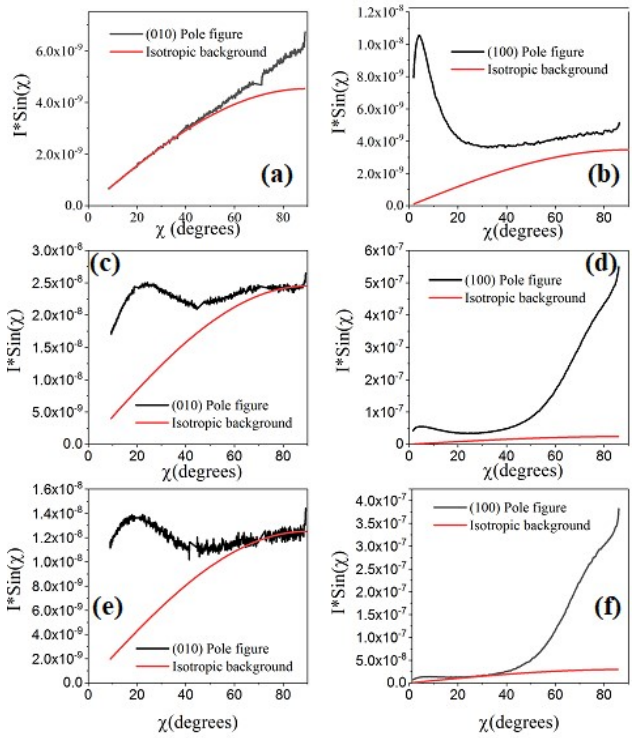

Figure S6. The pole figure analysis of the (a), (c), and (e) π-π stacking (010), and (b), (d), and (f) lamellar stacking (100) of the thin film.

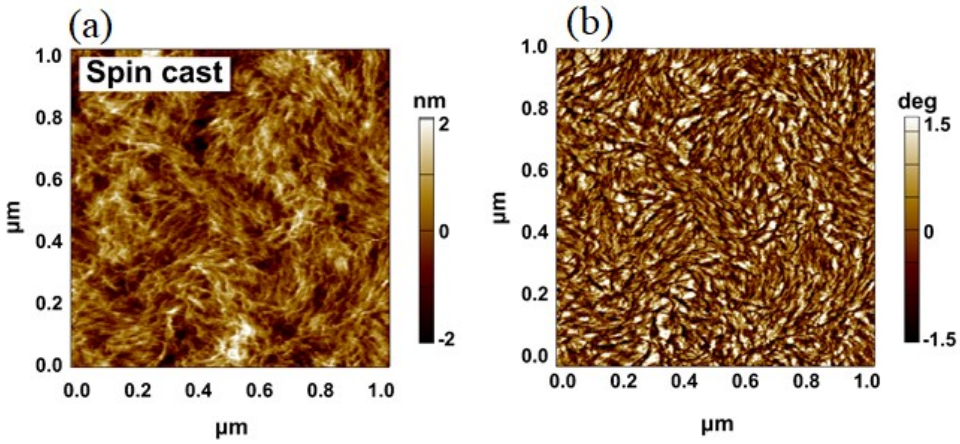

Figure S7. AFM image of spin-coated thin film (35 nm): (a) height image, (b) phase image.

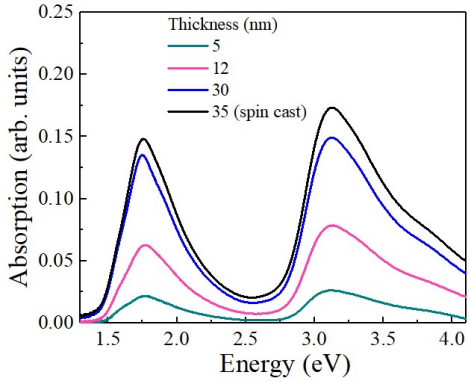

Figure S8**:** The UV-vis absorption spectra of N2200 films floated on the water. Three different thicknesses were characterized. The absorption of a spin-coated film (35 nm) is also included.